Thermoelectric properties of anisotropic semiconductors

W. E. Bies, R. J. Radtke,* and H. Ehrenreich
Physics Department and the Division of Engineering and Applied Sciences, Harvard University, Cambridge, Massachusetts 02138

E. Runge
AG Halbleitertheorie, Institut der Physik, Humboldt-Universität zu Berlin, Hausvogteiplatz 5-7, 10117 Berlin, Germany
(Received 14 November 2000; revised manuscript received 11 June 2001; published 8 February 2002)

General effective transport coefficients and the thermoelectric figure of merit ZT for anisotropic systems are derived. Sizable induced transverse fields on surfaces perpendicular to the current flow are shown to reduce the effective transport coefficients. A microscopic electronic model relevant for multivalleyed materials with parabolic bands is considered in detail. Within the effective-mass and relaxation-time approximations but neglecting the lattice thermal conductivity κ_l, the thermopower and Lorenz number are shown to be independent of the tensorial structure of the transport coefficients and are therefore isotropic. ZT is also isotropic for vanishing lattice thermal conductivity κ_l. A similar result holds in lower dimensions. For nonvanishing but sufficiently isotropic κ_l, ZT is ordinarily maximal along the direction of highest electrical conductivity σ. More general numerical calculations suggest that maximal ZT occurs along the principal direction with the largest σ/κ_l. An explicit bound on ZT is derived. Consideration of the Esaki-Tsu model shows that nonparabolic dispersion in superlattices has little effect on the thermopower at the carrier concentrations which maximize ZT. However, strong anisotropies develop when the chemical potential exceeds the miniband width.

DOI: 10.1103/PhysRevB.65.085208 PACS number(s): 72.20.Pa, 72.10.Bg

I. INTRODUCTION

In the search to find systems with large thermoelectric figures of merit ZT (for isotropic material $ZT=T\sigma S^2/\kappa$, where σ is the electrical conductivity, S is the Seebeck coefficient, and κ is the thermal conductivity), the emphasis has been more on new materials than on material structures or crystallographic anisotropy. Typical of new structures are superlattices, quantum wells,[1–8] and quantum wires.[9,10] It has been generally assumed that the direction of highest conductivity in an anisotropic material yields optimal thermoelectric properties. The correctness of this assumption is not obvious, since directions may exist along which the lattice thermal conductivity is abnormally low and the thermopower is high enough to result in large ZT even though the electrical conductivity is less than maximum.

Some effects of anisotropic transport tensors have been predicted and observed. Kelvin[11] predicted the existence of transverse temperature gradients due to off-diagonal terms in the thermal conductivity. They were observed by Borelius and Lindh,[12] Bridgman,[13] and Terada and Tsutsui.[14] Another anisotropic effect is the Bridgman or internal Peltier effect,[13,15] a contribution to the local evolution of heat that arises in nonuniform current flow. To the best of our knowledge, the consequences of these anisotropic effects in giving rise to transverse electric fields and temperature gradients have not been investigated previously.

This paper develops a more general microscopic transport theory of thermoelectricity in anisotropic systems. The ''highest-conductivity'' assumption is found to be correct for materials having simple band structures typically of the parabolic variety and essentially isotropic lattice thermal conductivities. However, the formalism developed here suggests more generally that the optimal orientation corresponds to the principal direction along which the ratio of the electronic to lattice thermal conductivity σ/κ_l is maximum. There are also several surprising results. These include the formation of possibly large induced transverse electric fields and temperature gradients, the fact that ZT is strictly isotropic in anisotropic systems having parabolic bands if the lattice thermal conductivity is neglected, and that a nearly isotropic thermopower and Lorenz number results under these conditions even if the bands are extremely anisotropic and nonparabolic.

The purpose of this paper is (i) to predict the effect of transverse induced fields in anisotropic materials, which should be observable experimentally without much difficulty, and (ii) to use the isotropy of the thermopower S and of ZT, which is predicted to hold in the limit when the lattice thermal conductivity, intervalley scattering, and nonparabolic bands can be neglected, as a reference frame for gauging the importance of nonzero lattice thermal conductivity and intervalley scattering.

The macroscopic formalism, based on the tensorial form of the usual phenomenological transport equations, is presented in Sec. II. The effects of sample boundaries for the rodlike geometry assumed throughout much of this paper are included by requiring that the transverse electric and heat currents vanish throughout the volume. Anisotropic and isotropic systems are shown to differ both qualitatively, through the presence of induced transverse fields, and quantitatively, through the magnitude of the transport coefficients.

More detailed statements concerning optimal orientations require use of a microscopic model. Section III introduces a model commonly used to study transport in semiconductors having multivalley, anisotropic parabolic band structures. The transport properties follow from the linearized Boltzmann equation in the effective-mass and relaxation-time approximations. Intervalley scattering is neglected. Somewhat surprisingly, the thermopower and Lorenz number turn out to

be isotropic. The same is true for ZT when the lattice thermal conductivity κ_l is neglected. Section III B shows that similar results hold for two- and one-dimensional systems. The realistic case corresponding to finite κ_l is considered in Sec. III C. If κ_l is sufficiently isotropic, the maximal ZT is shown to occur for samples cut along the direction of highest electrical conductivity. This rather unsurprising result, however, may be modified if the anisotropy of κ_l exceeds that of the electrical conductivity, leading to the conjecture concerning σ/κ_l mentioned above. An explicit expression for the upper bound on ZT is also derived, which is a generalization of that previously obtained[16] to anisotropic systems, and can serve as a guideline for the search for anisotropic high-ZT systems.

This microscopic description has been applied elsewhere to several materials of current interest.[17] The induced electric field and corresponding reduction of the effective electrical conductivity are shown in Ref. 17 to be important and potentially observable effects in bulk n-type Bi_2Te_3 and HgTe/HgCdTe superlattices (SL's). In HgTe/HgCdTe SL's the anisotropy is tunable by varying the composition and width of the barriers and wells. For sufficiently large anisotropy and for samples cut to a suitable angle with respect to the SL planes, the induced electric field can be as large as or greater than the external electric field.

The explicit effects of nonparabolicity and reduced bandwidth in superlattices on the thermopower and Lorenz number are investigated in Sec. IV. Both quantities remain nearly isotropic for small doping or carrier concentration. The thermopower is also bounded by its values along the principal axes, supporting the conjecture that optimal ZT is obtained along those directions.

II. ELECTRONIC TRANSPORT THEORY

We generalize conventional transport theory to anisotropic media in order to calculate the modified thermoelectric figure of merit. The tensor equations describing the transport of electrons and of heat in the presence of an electric field $\mathcal{E}$ and temperature gradient ∇T are

$$\mathbf{J}^e = \underline{L}^{11}\mathcal{E} + \underline{L}^{21}(-\nabla T/T), \tag{1}$$

$$\mathbf{J}^Q = \underline{L}^{12}\mathcal{E} + \underline{L}^{22}(-\nabla T/T). \tag{2}$$

Here $\mathbf{J}^e$ is the electric current density, $\mathbf{J}^Q$ is the heat current density, and $\underline{L}^{\alpha\beta}$ are the matrices of Onsager coefficients. With the notation $\underline{L}^{11}=\underline{\sigma}$ and $\underline{L}^{21}=T\underline{\sigma}\underline{S}$, where $\underline{\sigma}$ is the electrical conductivity tensor and $\underline{S}$ is the Seebeck tensor,[20] Eq. (1) becomes

$$\mathbf{J}^e = \underline{\sigma}(E - \underline{S}\nabla T) \equiv \underline{\sigma}\mathbf{F}. \tag{3}$$

Equation (2) can be put into the form[18,19]

$$\mathbf{J}^Q = \underline{\Pi}\mathbf{J}^e - \underline{\kappa}\nabla T \tag{4}$$

if we eliminate $\mathcal{E}$ in favor of $\mathbf{J}^e$, use the notation $\underline{L}^{12}=\underline{\Pi}\,\underline{\sigma}$, where $\underline{\Pi}$ is the Peltier tensor, and define the thermal conductivity tensor to be $\underline{\kappa}=(1/T)\underline{L}^{22}-\underline{\Pi}\,\underline{\sigma}\,\underline{S}$. As yet, we have not assumed the Onsager relations $\underline{L}^{\alpha\beta}=(\underline{L}^{\beta\alpha})^T$, which are equivalent to $\underline{\sigma}=\underline{\sigma}^T$, $\underline{\kappa}=\underline{\kappa}^T$, and $\underline{\Pi}=T\underline{S}^T$. These are not obviously applicable to a purely macroscopically described medium. Truesdell[21] has argued that, in crystalline solids of sufficiently low symmetry, $\underline{\kappa}$ may be nonsymmetric. His argument, however, relies only on group theory, and does not take into account the microscopic physics, in particular the fundamental principle of microscopic reversibility, on which the Onsager theory rests. A derivation of the Onsager relations from the linearized Boltzmann equation, in the natural frame for the problem given by the crystalline axes of an anisotropic solid, is given elsewhere (e.g., Ref. 22).

We shall assume that the crystal, whatever its anisotropy, is cut rectangularly.[20] Then Cartesian axes are defined and give the natural coordinate system in which to study the transport.

Transport in an anisotropic medium is modified by the presence of induced fields which arise via Eqs. (3) and (4) in response to the generalized forces resulting from, for example, the accumulation of charges on the surface of the sample. The induced fields are implicit in the treatment of Nye[20] (See Ch. 11, Sec. 2, p. 199); as shown there, end effects will be negligible if we assume that the length of the sample in the direction of transport (longitudinal) is large compared to the size of the transverse directions. In the rectangular samples under consideration here, the induced electric field will be uniform, except within a screening length away from the edges. Thus $\mathcal{E}=\mathcal{E}^{\rm ext}+\mathcal{E}^{\rm ind}$ and $\nabla T=\nabla T^{\rm ext}+\nabla T^{\rm ind}$ where $\mathcal{E}^{\rm ext}$ is the external applied electric field, $\mathcal{E}^{\rm ind}$ is the induced electric field, $\nabla T^{\rm ext}$ is the external applied temperature gradient, and $\nabla T^{\rm ind}$ is the induced temperature gradient. The fluxes $\mathbf{J}^e$ and $\mathbf{J}^Q$ generated by the total forces will therefore involve an induced part as well, and the net result is that, for a given applied force, the total flux will be smaller than would be the case in the absence of the induced fields. The induced fields vanish in samples cut along a principal axis of the conductivity tensor.

Consider an electric field $\mathcal{E}^{\rm ext}=(\mathcal{E}_\parallel,0,0)$ and temperature gradient $\nabla T^{\rm ext}=(\nabla_\parallel T,0,0)$ applied along the longitudinal ($\parallel$) direction. Let $\mathbf{F}=(F_x,F_y,F_z)=(F_\parallel,\mathbf{F}_\perp)$ with $F_\parallel$ the thermal and electric field along x, and $\mathbf{F}_\perp$ the induced transverse fields. We assume experimental conditions in which the transverse ($\perp$) electrical and thermal currents vanish throughout the volume. Then

$$\begin{pmatrix} J^e_\parallel \\ \mathbf{0} \end{pmatrix} = \underline{\sigma}\begin{pmatrix} F_\parallel \\ \mathbf{F}_\perp \end{pmatrix} = \begin{pmatrix} \sigma_\parallel & \underline{\sigma}^T_{od} \\ \underline{\sigma}_{od} & \underline{\sigma}_\perp \end{pmatrix}\begin{pmatrix} F_\parallel \\ \mathbf{F}_\perp \end{pmatrix} \tag{5}$$

and

$$\begin{pmatrix} J^Q_\parallel \\ \mathbf{0} \end{pmatrix} = \begin{pmatrix} TS_\parallel J^e_\parallel - \kappa_\parallel \nabla_\parallel T - \underline{\kappa}^T_{od}\nabla_\perp T \\ T\underline{S}^{(1)T}_{od} J^e_\parallel - \underline{\kappa}_{od}\nabla_\parallel T - \underline{\kappa}_\perp \nabla_\perp T \end{pmatrix}, \tag{6}$$

where $\sigma_\parallel$ is the component of the conductivity along the x direction, and $\underline{\sigma}_\perp$ is a 2×2 tensor for the transverse y,z directions. The 2×1 off-diagonal term $\underline{\sigma}_{od}$ and its transpose appear since the full conductivity tensor is not block diagonal. The tensor $\underline{\kappa}$ has a similar decomposition. We have invoked the Onsager relations in Eq. (6) by writing $\underline{\Pi}=T\underline{S}^T$. The Onsager relations also imply that the conductivity tensor

is symmetric, so that $\underline{\sigma}_\perp$ in Eq. (5) is symmetric as well. The same applies to the tensors $\underline{\kappa}$ and hence $\underline{\kappa}_\perp$ in Eq. (4). However, the Seebeck tensor

$$\underline{S}=\begin{pmatrix} S_\parallel & \underline{S}_{od}^{(1)} \\ \underline{S}_{od}^{(2)} & \underline{S}_\perp \end{pmatrix} \tag{7}$$

need not be symmetric.[23]

To calculate the electric conductivity we note that Eq. (5) leads to

$$\mathbf{F}_\perp = -\underline{\sigma}_\perp^{-1}\underline{\sigma}_{od}F_\parallel . \tag{8}$$

The off-diagonal elements of $\underline{\sigma}$ induce a current

$$J_\parallel^{\mathrm{e,ind}}=\underline{\sigma}_{od}^T\mathbf{F}_\perp=-\underline{\sigma}_{od}^T\underline{\sigma}_\perp^{-1}\underline{\sigma}_{od}F_\parallel \tag{9}$$

along the x direction. The total current

$$J_\parallel^e=J_\parallel^{e,\mathrm{ext}}+J_\parallel^{e,\mathrm{ind}}=(\sigma_\parallel-\underline{\sigma}_{od}^T\underline{\sigma}_\perp^{-1}\underline{\sigma}_{od})F_\parallel\equiv\sigma_1F_\parallel . \tag{10}$$

To calculate the effective thermal conductivity, we note that Eq. (6) yields the induced temperature gradients

$$\nabla_\perp T=\underline{\kappa}_\perp^{-1}(T\underline{S}_{od}^{(1)T}J_\parallel^e-\underline{\kappa}_{od}\nabla_\parallel T). \tag{11}$$

Substituting back into Eq. (6) gives

$$J_\parallel^{Q,\mathrm{ind}}=-\underline{\kappa}_{od}^T\nabla_\perp T=-\underline{\kappa}_{od}^T\underline{\kappa}_\perp^{-1}(T\underline{S}_{od}^{(1)T}J_\parallel^e-\underline{\kappa}_{od}\nabla_\parallel T), \tag{12}$$

whence

$$\begin{aligned} J_\parallel^Q&=T(S_\parallel-\underline{\kappa}_{od}^T\underline{\kappa}_\perp^{-1}\underline{S}_{od}^{(1)T})J_\parallel^e-(\kappa_\parallel-\underline{\kappa}_{od}^T\underline{\kappa}_\perp^{-1}\underline{\kappa}_{od})\nabla_\parallel T \\ &\equiv TS_{\mathrm{eff}}J_\parallel^e-\kappa_{\mathrm{eff}}\nabla_\parallel T \ , \end{aligned} \tag{13}$$

where S_{eff} and κ_{eff} are ''effective'' transport coefficients to be discussed further below. Observe that σ_1, Eq. (10), and κ_{eff}, Eq. (13), have the same form. Since $\underline{\sigma}_\perp$ and $\underline{\sigma}_\perp^{-1}$ have positive eigenvalues, the quadratic form $\underline{\sigma}_{od}^T\underline{\sigma}_\perp^{-1}\underline{\sigma}_{od}$ is positive definite. Thus, the induced current opposes the external current $J_\parallel^{e,\mathrm{ext}}=\sigma_\parallel F_\parallel$. The induced fields therefore lead to a reduced conductivity: $\sigma_1\leqslant\sigma_\parallel$. If $\underline{S}$ is diagonal, σ_1 is the effective conductivity; otherwise, the induced temperature gradients give rise to additional terms considered below. In the isotropic case, the induced fields vanish, and $\sigma_1=\sigma_\parallel$. Note that in general $\sigma_1\geqslant 0$ because $\sigma_1F_\parallel^2=J_\parallel^eF_\parallel=\mathbf{F}^T\cdot\mathbf{J}^e=\mathbf{F}^T\cdot\underline{\sigma}\cdot\mathbf{F}\geqslant 0$. As in the case of σ_1, the induced temperature gradients produce an induced heat current along x which opposes the external heat current $-\kappa_\parallel\nabla_\parallel T$. The net result is a reduced effective thermal conductivity: $0\leqslant\kappa_{\mathrm{eff}}\leqslant\kappa_\parallel$.

Returning to Eq. (10), we have

$$F_\parallel=(\mathcal{E}_\parallel-S_\parallel\nabla_\parallel T-\underline{S}_{od}^{(1)}\nabla_\perp T). \tag{14}$$

Substituting Eq. (11) into Eq. (14) leads with the help of Eq. (10) to

$$\begin{aligned} J_\parallel^e&=\frac{\sigma_1}{1+\sigma_1T\underline{S}_{od}^{(1)}\underline{\kappa}_\perp^{-1}\underline{S}_{od}^{(1)T}}(\mathcal{E}_\parallel-(S_\parallel-\underline{S}_{od}^{(1)}\underline{\kappa}_\perp^{-1}\underline{\kappa}_{od})\nabla_\parallel T) \\ &\equiv\sigma_{\mathrm{eff}}(\mathcal{E}_\parallel-S_{\mathrm{eff}}\nabla_\parallel T). \end{aligned} \tag{15, 16}$$

From the properties of σ_1, $0\leqslant\sigma_{\mathrm{eff}}\leqslant\sigma_\parallel$. Therefore, induced fields and temperature gradients always reduce the effective conductivity. Also, S_{eff} in Eq. (16) is the same as S_{eff} in Eq. (13) because $\underline{\kappa}_\perp$ and hence $\underline{\kappa}_\perp^{-1}$ are symmetric.

The results of Eqs. (13) and (16) are of importance because they show that in an anisotropic crystal the parallel component of the electronic current can still be expressed by an expression having the form of Eqs. (3) and (4) but with all transport coefficients replaced by effective quantities σ_{eff}, κ_{eff}, and S_{eff}.

In the steady state, Domenicali's continuity equation for the energy density in an anisotropic medium, as obtained by generalizing Mahan's treatment,[19] reads

$$\mathbf{J}^e\underline{\sigma}^{-1}\mathbf{J}^e+\nabla\cdot(\underline{\kappa}\nabla T)=0. \tag{17}$$

It can be shown that this reduces to

$$\sigma_{\mathrm{eff}}^{-1}J_\parallel^{e2}+\kappa_{\mathrm{eff}}\nabla_\parallel^2T=0. \tag{18}$$

The thermoelectric figure of merit becomes

$$ZT=T\sigma_{\mathrm{eff}}S_{\mathrm{eff}}^2/\kappa_{\mathrm{eff}}, \tag{19}$$

with the help of Eqs. (16), (13), and (18). The form of ZT remains the same, but again the transport coefficients are simply replaced by their effective versions.

III. MICROSCOPIC MODEL: PARABOLIC BANDS

A. Three-dimensional structures

According to semiclassical transport theory, the Boltzmann equation in the relaxation-time approximation yields the electronic transport coefficients

$$\sigma_{ij}=e^2\int d\varepsilon(-\partial f_0/\partial\varepsilon)\Sigma_{ij}(\varepsilon), \tag{20}$$

$$T(\sigma\cdot S)_{ij}=e\int d\varepsilon(-\partial f_0/\partial\varepsilon)\Sigma_{ij}(\varepsilon)(\varepsilon-\mu), \tag{21}$$

$$T\kappa_{0,ij}=\int d\varepsilon(-\partial f_0/\partial\varepsilon)\Sigma_{ij}(\varepsilon)(\varepsilon-\mu)^2, \tag{22}$$

where f_0 is the Fermi-Dirac distribution $f_0(\varepsilon)=1/\{\exp[(\varepsilon-\mu)/k_BT]+1\}$, μ the chemical potential, and

$$\Sigma_{ij}(\varepsilon)=\int\frac{2d^3\mathbf{k}}{(2\pi)^3}v_i(\mathbf{k})\sum_l\tau_{jl}(\mathbf{k})v_l(\mathbf{k})\delta[\varepsilon-\varepsilon(\mathbf{k})] \tag{23}$$

are the components of the transport distribution tensor, the generalization of the function discussed by Mahan and Sofo.[16] Here $\varepsilon(\mathbf{k})$ is the electronic dispersion relation, $v_i(\mathbf{k})=\hbar^{-1}\partial\varepsilon(\mathbf{k})/\partial k_i$ the electronic group velocity, and

$\underline{\tau}(\mathbf{k})$ the relaxation time. In keeping with the standard literature[24] and cyclotron resonance experiments[25] in Si and Ge, the relaxation time is an anisotropic tensor. For the sake of simplicity we shall assume that the matrix elements of $\underline{\tau}$ depend on $\mathbf{k}$ only through the energy and that they all have the same energy dependence; i.e., $\tau_{ij}(\mathbf{k})=\tau[\varepsilon(\mathbf{k})]U_{ij}$ where $\underline{U}$ is a constant dimensionless matrix. This form is as general as required in the papers cited above.[24,25]

Note that $\underline{\kappa}_0$ is the electronic thermal conductivity at zero electrochemical potential gradient inside the sample;[16] the usual electronic thermal conductivity at zero electric current, $\underline{\kappa}_e$, is given in terms of $\underline{\kappa}_0$ by $\underline{\kappa}_e=\underline{\kappa}_0-T\underline{S}^T\underline{\sigma}\,\underline{S}$. The lattice conductivity, κ_l, is not considered in this section.

The microscopic model to be used here assumes the conduction to be taking place in a single band having N degenerate parabolic valleys centered at $\mathbf{k}^{(n)}, n=1,\ldots,N$, respectively. The dispersion relation for each valley is

$$\varepsilon^{(n)}(\mathbf{k})=\varepsilon_0+(\hbar^2/2)\sum_{i,j}(k_i-k_i^{(n)})M_{ij}^{(n)-1}(k_j-k_j^{(n)}) \tag{24}$$

with $\underline{M}^{(n)-1}$ the inverse effective-mass tensor. The corresponding group velocity is

$$v_i^{(n)}(\mathbf{k})=\hbar^{-1}\partial\varepsilon(\mathbf{k})/\partial k_i=\hbar\sum_j M_{ij}^{(n)-1}(k_j-k_j^{(n)}). \tag{25}$$

Intervalley scattering will be neglected. Thus the transport distribution tensor involves just a sum over the N valleys. Then independent of crystal orientation we have

$$\Sigma_{ij}(\varepsilon)=\tau(\varepsilon)\sum_{n=1}^{N}\int\frac{2d^3\mathbf{k}}{(2\pi)^3}\hbar^2\sum_{i',j',l}M_{ii'}^{(n)-1}k_{i'}U_{jj'}^{(n)}M_{j'l}^{(n)-1}\times k_l\delta[\varepsilon-\varepsilon(\mathbf{k}+\mathbf{k}^{(n)})] \tag{26}$$

$$=\tau(\varepsilon)\hbar^2\sum_{n=1}^{N}\sum_{i'j'l}M_{ii'}^{(n)-1}U_{jj'}^{(n)}M_{j'l}^{(n)-1}\times\int k_{i'}k_l\delta(\varepsilon-\mathbf{k}\underline{X}^{(n)}\mathbf{k})\frac{2d^3\mathbf{k}}{(2\pi)^3} \tag{27}$$

$$=[2\tau(\varepsilon)\hbar^2/(2\pi)^3]\times\sum_{n=1}^{N}\sum_{i'j'l}M_{ii'}^{(n)-1}U_{jj'}^{(n)}M_{j'l}^{(n)-1}\times\left[-\frac{\partial}{\partial X_{i'l}^{(n)}}\int\Theta(\varepsilon-\mathbf{k}\underline{X}^{(n)}\mathbf{k})d^3\mathbf{k}\right] \tag{28}$$

$$=[2^{3/2}\tau(\varepsilon)\varepsilon^{3/2}/3\pi^2\hbar^3]\times\sum_{n=1}^{N}\sum_{l}\sqrt{\det\underline{M}^{(n)}}U_{jl}^{(n)}M_{li}^{(n)-1}, \tag{29}$$

where $X_{ij}^{(n)}$ are the components of $\underline{X}^{(n)}=(\hbar^2/2)\underline{M}^{(n)-1}$. This transformation relies explicitly on the validity of the effective-mass approximation, the neglect of intervalley scattering, and the relaxation-time approximation used here. The terms inside the square brackets in Eq. (28) are evaluated using the identity

$$\frac{\partial}{\partial X_{ij}^{(n)}}\det\underline{X}^{(n)}=(\det\underline{X}^{(n)})X_{ij}^{(n)-1} \tag{30}$$

and the change of variable $\mathbf{k}'=\sqrt{\underline{X}^{(n)}}\mathbf{k}$. Thus,

$$\underline{\Sigma}(\varepsilon)=\underline{A}\mathcal{T}(\varepsilon) \tag{31}$$

with

$$\underline{A}=\sum_{n=1}^{N}(m_0^{-1/2}\sqrt{\det\underline{M}^{(n)}})(\underline{U}^{(n)}\underline{M}^{(n)-1})^T \tag{32}$$

and

$$\mathcal{T}(\varepsilon)=\frac{2^{3/2}m_0^{1/2}}{3\pi^2\hbar^3}\varepsilon^{3/2}\tau(\varepsilon). \tag{33}$$

The constant, dimensionless matrix $\underline{A}$ contains the full tensorial structure associated with the crystal symmetry and separates it from the energy dependence in $\mathcal{T}(\varepsilon)$.

The conductivity then becomes

$$\underline{\sigma}=e^2\int d\varepsilon(-\partial f_0/\partial\varepsilon)\mathcal{T}(\varepsilon)\underline{A}\equiv\sigma_0\underline{A}. \tag{34}$$

For silicon and germanium this expression reduces to that given by Smith *et al.*[26]

The Seebeck tensor is therefore necessarily *isotropic* since

$$\underline{\sigma}\,\underline{S}=(e/T)\int d\varepsilon(-\partial f_0/\partial\varepsilon)\mathcal{T}(\varepsilon)(\varepsilon-\mu)\underline{A}\equiv\underline{A}\sigma_0S_0, \tag{35}$$

$$\underline{S}=\underline{\sigma}^{-1}\,\underline{\sigma}\,\underline{S}=S_0\underline{1}. \tag{36}$$

Further, using Eqs. (23) and (32), $\underline{\kappa}_0=\underline{A}\kappa_0$ and hence

$$\underline{\kappa}_e=\underline{\kappa}_0-T\underline{S}^T\underline{\sigma}\,\underline{S}\equiv\underline{A}\kappa_e \tag{37}$$

for $\kappa_e=\kappa_0-T\sigma_0S_0^2$.

These results lead to the following surprising conclusion: When the lattice thermal conductivity is neglected, then, within the effective-mass approximation as specified here, the thermoelectric figure of merit ZT is independent of the sample orientation. Note that

$$\underline{\kappa}_e\cdot\underline{\sigma}^{-1}=\underline{A}\kappa_e\cdot\underline{A}^{-1}/\sigma_0=(\kappa_e/\sigma_0)\underline{1}\equiv L_0T\underline{1}, \tag{38}$$

where the Lorenz number $L_0=\kappa_e/\sigma_0T$. Thus, $\kappa_{e,ij}=L_0T\sigma_{ij}$ and $\kappa_{\text{eff}}=L_0T\sigma_{\text{eff}}$ as expected. Finally, since $\underline{S}$ is isotropic, $S_{\text{eff}}=S_0$. Combining these effective transport coefficients yields

$$ZT=T\sigma_{\text{eff}}S_{\text{eff}}^2/\kappa_{\text{eff}}=S_0^2/L_0, \tag{39}$$

a constant independent of direction. The isotropy is lost if either a nonzero lattice thermal conductivity or nonzero intervalley scattering is included. Thus, $\kappa_l=0$ with no intervalley scattering provides a baseline; for typical thermoelectic materials the lattice thermal conductivity and intervalley

scattering will be small and hence by Eq. (39) the figure of merit ZT will be less anisotropic than naively expected.

B. Lower-dimensional structures

Dimensionality enters the transport coefficients through the **k**-space integrals d^3k, $(2\pi/L_z)d^2k$, and $[(2\pi)^2/L_yL_z]dk$ for three, two, or one dimensions, respectively, where L_y and L_z are the sample sizes in the y and z directions. Dimensionality also enters through the confinement energies and effective masses for carriers constrained to move in a lower-dimensional system.

For the two-dimensional case with $E=(\mathcal{E}_\parallel,\mathcal{E}_\perp)$ and $\nabla T=(\nabla_\parallel T,\nabla_\perp T)$, the induced fields are given by Eqs. (8) and (11), and the transport coefficients by Eqs. (13) and (16) with $\underline{\sigma}_\perp$ replaced by σ_{yy}, and $\underline{\sigma}_{od}$ replaced by σ_{yx}; it is similar for the other transport coefficients. The analogue of Eq. (23) for the components of the transport distribution tensor is obtained within the effective-mass approximation:

$$\Sigma_{ij}(\varepsilon)=\frac{2\tau(\varepsilon)\hbar^2}{4\pi^2L_z}\sum_{n=1}^{N}\sum_{i'j'_l}M_{ii'}^{(n)-1}U_{jj'}^{(n)}M_{j'l}^{(n)-1}\times\int d^2\mathbf{k}k_{i'}k_l\delta(\varepsilon-\mathbf{k}\underline{X}^{(n)}\mathbf{k}). \tag{40}$$

This expression has the same form as Eq. (31) with

$$\underline{A}=\sum_{n=1}^{N}\sqrt{\det\underline{M}^{(n)}}(\underline{U}^{(n)}\underline{M}^{(n)-1})^T \tag{41}$$

and

$$\mathcal{T}(\varepsilon)=\varepsilon\tau(\varepsilon)/\pi\hbar^2L_z. \tag{42}$$

These equations are to be compared with Eqs. (32) and (33) for the three-dimensional case. Thus, analogously to Eqs. (34), (36), and (37), $\underline{\sigma}=\underline{A}\sigma_0$, $\underline{S}=S_0\underline{1}$, and $\underline{\kappa}_e=\underline{A}\kappa_e$ where the two-dimensional $\underline{A}$ and $\overline{\mathcal{T}}(\varepsilon)$ must be used in defining σ_0, S_0, and κ_0. Finally, $\underline{\kappa}_e\underline{\sigma}^{-1}=L_0T\underline{1}$ so that $\kappa_{\rm eff}=L_0T\sigma_{\rm eff}$. Also, $S_{\rm eff}=S_0$ because $\underline{S}$ is isotropic in two dimensions as well. The corresponding figure of merit $ZT=T\sigma_{\rm eff}S_{\rm eff}^2/\kappa_{\rm eff}=S_0^2/L_0$ is again independent of direction, as in three dimensions.

It is seen that the two-dimensional and three-dimensional results are entirely analogous and that the former are obtained from the latter by taking the limit as one of the effective masses tends to infinity. In this limit, the ellipsoidal surface in **k** space of constant energy becomes increasingly prolate, until it reaches the edge of the Brillouin zone, after which it assumes a cylindrical shape extending from $-\pi/L_z$ to π/L_z upon further increase in the effective-mass parameter. Furthermore ZT in two dimensions can be enhanced due to the factor of $1/L_z$ in the density of states, which, as pointed out in Ref. 1, becomes large for small thicknesses.

In the one-dimensional case there is no transport in the transverse direction. Thus there are no transverse fields and the microscopic and effective transport coefficients are the same. Moreover, all transport coefficients are scalar. The transport distribution function is found to be

$$\Sigma(\varepsilon)=\sum_{n=1}^{N}\frac{2}{\pi L_yL_z}\sqrt{\frac{2\varepsilon}{\hbar^2m_x^{(n)}}}\tau(\varepsilon). \tag{43}$$

Just as in two dimensions, the $1/L_yL_z$ factor leads to an enhancement of the density of states and thus of ZT for thin wires.[9]

C. Implications for ZT

We shall now derive an upper bound for ZT of the Mahan and Sofo form[16] and show that the highest-conductivity direction gives optimal values for ZT. An *isotropic* lattice thermal conductivity κ_l, which causes ZT to lose its isotropy, will now be included.

The figure of merit including an isotropic lattice thermal conductivity $\underline{\kappa}_l=\kappa_l\underline{1}$ may be written in the form of Eq. (19) where $\sigma_{\rm eff}$ and $S_{\rm eff}$ are as in Sec. II and $\kappa_{\rm eff}=\kappa_e^*+\kappa_l$. Let

$$\underline{\kappa}_e=\begin{pmatrix}\kappa_\parallel & \underline{\kappa}_{od}^T\\ \underline{\kappa}_{od} & \underline{\kappa}_\perp\end{pmatrix} \tag{44}$$

and [in analogy with Eq. (13)]

$$\kappa_e^*=\kappa_\parallel-\underline{\kappa}_{od}^T(\underline{\kappa}_\perp+\kappa_l\underline{1})^{-1}\underline{\kappa}_{od}. \tag{45}$$

κ_e^* defines the electronic thermal conductivity in the presence of the nonvanishing κ_l and the sample boundaries. As shown in the Appendix, the upper bound on ZT is given by

$$ZT\leqslant a_0\kappa_0/\kappa_l. \tag{46}$$

The dimensionless quantity a_0 is defined by Eq. (A2). In the isotropic case,[16] $a_0=1$; in the present case, a_0 is of order unity. The maximum value is obtained when the parameter ξ, as defined by Eq. (A12), approaches unity. This is the case if and only if $\mathcal{T}(\varepsilon)$ is proportional to a δ function. In the more physical case, $\mathcal{T}(\varepsilon)\propto\varepsilon^r$ with r varying between -0.5 and 2, which encompasses many of the common scattering mechanisms in semiconductors. Numerical computations show that ξ tends to 1 as $\mu/k_BT\to-\infty$ and to zero as $\mu/k_BT\to\infty$. For $\mu/k_BT=0$, ξ ranges from 0.5 to 0.8. Thus, the upper bound at $\xi=1$ can be reached at the cost of going to low carrier concentrations, whereas higher carrier concentrations imply smaller ξ.

We now show that, in the effective-mass, relaxation-time, no intervalley scattering, and isotropic-thermal-conductivity approximations, ZT is highest in the direction of maximum electrical conductivity. In the anisotropic case, $\sigma_{\rm eff}$ and $\kappa_{\rm eff}$ have an angular dependence. $S_{\rm eff}$ does not because in our microscopic model $\underline{S}$ is isotropic. ZT is therefore also anisotropic. Now let $\underline{P}$ be any symmetric and positive matrix and $\lambda\geqslant0$ a positive number; then by the properties of positive matrices, $\underline{P}^{-1}\geqslant(\underline{P}+\lambda\underline{1})^{-1}$. $\underline{P}=\underline{\kappa}_\perp$ and $\lambda=\kappa_l$. Thus

$$\underline{\kappa}_{od}^T(\underline{\kappa}_\perp+\kappa_l\underline{1})^{-1}\underline{\kappa}_{od}\leqslant\underline{\kappa}_{od}^T\underline{\kappa}_\perp^{-1}\underline{\kappa}_{od} \tag{47}$$

and consequently for any κ_l,

$$\kappa_e^*(\kappa_l) \geqslant \kappa_e^*(\kappa_l=0) = (\kappa_e/\sigma_0)\sigma_{\text{eff}}. \tag{48}$$

This shows that the ratio $\kappa_e^*/\sigma_{\text{eff}}$ is minimized when the axis of current flow in the steady state lies along one of the principal directions, where, whatever the value of κ_l, the induced-field related terms vanish and so equality is obtained in Eq. (48). Writing ZT in the form

$$ZT = \frac{S_0^2}{\kappa_e^*/T\sigma_{\text{eff}} + \kappa_l/T\sigma_{\text{eff}}}, \tag{49}$$

the second term in the denominator is seen to be smallest along the principal direction with largest electrical conductivity. Therefore ZT is maximized for current flow along this direction.

By contrast, for a sufficiently anisotropic lattice thermal conductivity the favored direction might be determined by κ_l's minimum rather than that of the highest electrical conductivity. For crystals in which two of the principal values of the electrical conductivity are equal, such as Bi_2Te_3 and SL's, numerical results show that as long as the anisotropy of $\underline{\kappa_l}$ is smaller than that of $\underline{\sigma}$, the optimum ZT is still to be found in the direction of greatest electrical conductivity. This suggests that, generally speaking, the figure of merit will be maximized in the principal crystal direction in which the ratio $\sigma_i/\kappa_{l,i}$ is greatest, where σ_i and $\kappa_{l,i}$ are the principal values of the electrical and lattice thermal conductivity tensors obtained from summing over valleys.

IV. MICROSCOPIC MODEL: NONPARABOLIC BANDS

Within the effective-mass approximation, the analysis of Sec. III showed that the thermopower and Lorenz number are isotropic when the lattice thermal conductivity is neglected. To see how a nonparabolic band structure affects these conclusions, consider an electronic dispersion relation of the Esaki-Tsu form:[27]

$$\varepsilon(\mathbf{k}) = \hbar^2 k_\parallel^2/2m_\parallel + \Delta(1-\cos k_z d) \tag{50}$$

with wave vector $\mathbf{k}=(k_\parallel\cos\varphi, k_\parallel\sin\varphi, k_z)$. This relation models a superlattice of period d. The in-plane dispersion is parabolic with mass $m_\parallel$, and that along the growth direction z has a tight-binding form with bandwidth $2\Delta=[\varepsilon(0,0,\pi/d) - \varepsilon(0,0,0)]$. Since the mass along the growth direction $m_z = \hbar^2/\Delta d^2$, the anisotropy can be increased by reducing Δ.

In the principal frame of the SL, the transport distribution tensor [Eq. (23)] is diagonal with components

$$\Sigma_{\text{growth}}(\varepsilon) = \frac{m_\parallel d\,\tau(\varepsilon)}{2\pi^2\hbar^4} \times \begin{cases} \Delta^2\cos^{-1}(1-\varepsilon/\Delta) + (\varepsilon-\Delta)\sqrt{\varepsilon(2\Delta-\varepsilon)}, & \varepsilon < 2\Delta, \\ \pi\Delta^2, & \varepsilon \geqslant 2\Delta \end{cases} \tag{51}$$

along the growth direction and

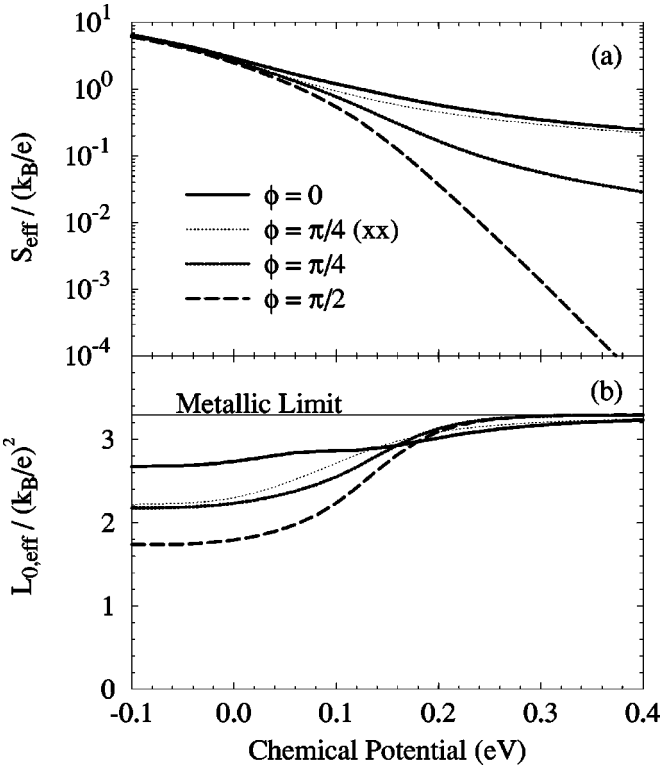

FIG. 1. (a) Effective thermopower S_{eff} and (b) effective Lorenz number $L_{0,\text{eff}}=\kappa_{\text{eff}}/\sigma_{\text{eff}}T$ as a function of chemical potential for the superlattice described in Sec. IV, neglecting lattice thermal conductivity. Shown are samples cut along $\phi=0$ (heavy solid line), $\pi/4$ (heavy dotted line), and $\pi/2$ (heavy dashed line) where ϕ is the angle between the direction of maximum conductivity $\sigma_{\max}$ and the external field E^{ext}. The results for $\phi=\pi/4$ neglecting the effects of the induced fields are also presented (light dotted line), labeled by (xx) in the legend. The metallic limit of $L_0/(k_B/e)^2=\pi^2/3$ is indicated in (b).

$$\Sigma_{\text{in plane}}(\varepsilon) = \frac{\tau(\varepsilon)}{\pi^2\hbar^2 d} \times \begin{cases} (\varepsilon-\Delta)\cos^{-1}(1-\varepsilon/\Delta) + \sqrt{\varepsilon(2\Delta-\varepsilon)}, & \varepsilon < 2\Delta, \\ \pi(\varepsilon-\Delta), & \varepsilon \geqslant 2\Delta \end{cases} \tag{52}$$

along the planes. The transport coefficients are obtained from Eqs. (20)–(22) in the principal frame and then transformed into the sample frame. As in Sec. III, the relaxation time $\tau(\mathbf{k})$ is assumed to be a function of energy only. Direct computation with $\tau \propto \varepsilon^r$ indicates that the qualitative features discussed below are independent of the choice of r. Quantitatively, the thermopower is an approximately linear function of r at fixed sample orientation and chemical potential μ and increases by approximately 50% as r goes from 0 to 1.5. In what follows, $r=0$, $d=100$ Å, $m_\parallel/m_0=0.021$, and $\Delta=57$ meV, corresponding to the $C1$ subband in a 50-Å $Hg_{0.75}Cd_{0.25}Te$/50-Å $Hg_{0.7}Cd_{0.3}Te$ SL.

The anisotropy in the resulting effective thermopower $S_{\rm eff}$ [Eq. (13)] and Lorenz number $L_{0,\rm eff}=\kappa_{\rm eff}/\sigma_{\rm eff}T$ is shown in Fig. 1. For $\mu<0$, $S_{\rm eff}$ along the growth and in-plane directions differ by $<10\%$. This near isotropy is expected, since the carriers determining $S_{\rm eff}$ are near the zone center, where the effective-mass approximation is good. The anisotropy increases substantially as μ increases past 2Δ, a region where the bands are appreciably nonparabolic, reaching over 6000 at $\mu=0.4$ eV. From Fig. 1(b), the anisotropy in $L_{0,\rm eff}$ is at most 30% and goes to zero in the large-μ limit, approaching the metallic value of $(\pi^2/3)(k_B/e)^2$. As ZT for this band structure is maximal for $\mu\sim 0$, the anisotropies in $S_{\rm eff}$ and $L_{0,\rm eff}$ in the relevant parameter range are small.

ACKNOWLEDGMENTS

We thank Frans Spaepen for helpful discussions. This work was supported by DARPA through ARL Contract No. DAAD17-00-C-0134 and the National Science Foundation through Grant No. CHE9610501.

APPENDIX

We present here a derivation of an upper bound of the Mahan and Sofo form[16] for an anisotropic material. From $\underline{\sigma}=\underline{A}\sigma_0$ [see Eq. (35)] we infer

$$\sigma_{\rm eff}=\sigma_0 a_0 \tag{A1}$$

with

$$a_0=A_{xx}-A_{xy}\frac{A_{yx}A_{zz}-A_{yz}A_{zx}}{A_{yy}A_{zz}-A_{yz}A_{zy}}-A_{xz}\frac{A_{zx}A_{yy}-A_{zy}A_{yx}}{A_{zz}A_{yy}-A_{yz}A_{zy}}. \tag{A2}$$

When the κ_l dependence in Eq. (45) is taken into account, we find similarly

$$\kappa_e^*=\kappa_e a(\kappa_l) \tag{A3}$$

with $a(\kappa_l=0)=a_0$ and

$$a(\kappa_l)=A_{xx}-A_{xy}\frac{A_{yx}(A_{zz}+\kappa_l/\kappa_e)-A_{yz}A_{zx}}{(A_{yy}+\kappa_l/\kappa_e)(A_{zz}+\kappa_l/\kappa_e)-A_{yz}A_{zy}} -A_{xz}\frac{A_{zx}(A_{yy}+\kappa_l/\kappa_e)-A_{zy}A_{yx}}{(A_{yy}+\kappa_l/\kappa_e)(A_{zz}+\kappa_l/\kappa_e)-A_{yz}A_{zy}}. \tag{A4}$$

Therefore

$$ZT=\frac{T\sigma_0 S_0^2 a_0}{(\kappa_0-T\sigma_0 S_0^2)a(\kappa_l)+\kappa_l}. \tag{A5}$$

Following Mahan and Sofo, we introduce dimensionless integrals

$$I_n=\int_{-\mu/k_BT}^{\infty}dx\frac{e^x}{(e^x+1)^2}s(x)x^n,\quad s(x)=\hbar r_0\mathcal{T}(\mu+xkT), \tag{A6}$$

where r_0 is the Bohr radius. In terms of these moments,

$$\sigma_0=\tilde{\sigma}_0 I_0, \tag{A7}$$

$$\sigma_0 S_0=(k_B/e)\tilde{\sigma}_0 I_1, \tag{A8}$$

$$\kappa_0=(k_B/e)^2 T\tilde{\sigma}_0 I_2, \tag{A9}$$

where $\tilde{\sigma}_0=e^2/\hbar r_0$ has dimensions of conductivity. Then

$$ZT=\frac{\tilde{\alpha}I_1^2/I_0}{(\tilde{\alpha}I_2-\tilde{\alpha}I_1^2/I_0)a(\kappa_l)/a_0+1/a_0} \tag{A10}$$

$$=\frac{\xi}{(1-\xi)a(\kappa_l)/a_0+B} \tag{A11}$$

with $\tilde{\alpha}=(k_B/e)^2T\tilde{\sigma}_0/\kappa_l$,

$$\xi=I_1^2/I_0 I_2, \tag{A12}$$

and $B=1/\tilde{\alpha}I_2 a_0=\kappa_l/\kappa_0 a_0$. By the Cauchy-Schwarz inequality, $0\leqslant\xi\leqslant 1$. The limit as ξ tends to 1 maximizes the figure of merit by maximizing the numerator and minimizing the denominator in Eq. (A11). From Eq. (A4) it may be seen that for $\kappa_l/\kappa_e=\kappa_l/(k_B/e)^2T\tilde{\sigma}_0 I_2(1-\xi)$ sufficiently large, $a(\kappa_l)$ tends to A_{xx}, and certainly this condition is met as $1-\xi$ tends to zero. Thus as $\xi\to 1$ we have that

$$ZT\to\frac{\xi}{(1-\xi)A_{xx}/a_0+B}\leqslant\frac{1}{B}=\frac{\kappa_0 a_0}{\kappa_l}. \tag{A13}$$

*Present address: Schlumberger, Sugar Land Product Center, 110 Schlumberger Dr., MD110-4, Sugar Land, TX 77478.

[1] L. D. Hicks and M. S. Dresselhaus, Phys. Rev. B **47**, 12 727 (1993).
[2] G. D. Mahan and H. B. Lyon, Jr., J. Appl. Phys. **76**, 1899 (1994).
[3] J. O. Sofo and G. D. Mahan, Appl. Phys. Lett. **65**, 2690 (1994).
[4] D. A. Broido and T. L. Reinecke, Phys. Rev. B **51**, 13 797 (1995).
[5] L. D. Hicks, T. C. Harman, X. Sun, and M. S. Dresselhaus, Phys. Rev. B **53**, R10 493 (1996).
[6] D. A. Broido and T. L. Reinecke, Appl. Phys. Lett. **70**, 2834 (1997); (unpublished).
[7] L. D. Hicks,T. C. Harman, and M. S. Dresselhaus, Appl. Phys. Lett. **63**, 3230 (1993).
[8] D. A. Broido and T. L. Reinecke, Appl. Phys. Lett. **67**, 1170 (1995).
[9] L. D. Hicks and M. S. Dresselhaus, Phys. Rev. B **47**, 16 631 (1993).
[10] D. A. Broido and T. L. Reinecke, Appl. Phys. Lett. **67**, 100 (1995).
[11] W. Thomson, Trans. - R. Soc. Edinbrgh **21**, 153 (1857).
[12] G. Borelius and A. E. Lindh, Ann. Phys. (Leipzig) **53**, 97 (1917).
[13] P. W. Bridgman, Proc. Natl. Acad. Sci. U.S.A. **13**, 46 (1927). See also P. W. Bridgman, *The Thermodynamics of Electrical Phenomena in Metals and a Condensed Collection of Thermody-*

namic Formulas (Dover, New York, 1961), Chap. 4.
[14] T. Terada and T. Tsutsui, Proc. Imp. Acad. (Tokyo) **3**, 132 (1927).
[15] P. Ehrenfest and A. J. Rutgers, Proc. Amst. Acad. **32**, 698 (1929); **32**, 883 (1929).
[16] G. D. Mahan and J. O. Sofo, Proc. Natl. Acad. Sci. U.S.A. **93**, 7436 (1996).
[17] W. E. Bies, R. J. Radtke, and H. Ehrenreich, J. Appl. Phys. **86**, 5065 (1999).
[18] H. Jones, in *Handbuch der Physik*, (Springer-Verlag, New York, 1956), Vol. 19, p. 227.
[19] G. D. Mahan, in *Solid State Physics*, edited by H. Ehrenreich and F. Spaepen (Academic, New York, 1998), Vol. 51.
[20] This relation defines $\underline{S}$ and agrees with the definition of thermopower given in J. F. Nye, *Physical Properties of Crystals: Their Representation by Tensors and Matrices* (Oxford University Press, London, 1957), Chap. 12, Sec. 3, p. 225.
[21] C. Truesdell, *Rational Thermodynamics: A Course of Lectures on Selected Topics* (McGraw-Hill, New York, 1969).
[22] W. E. Bies, Ph.D. thesis, Harvard University, 2000, Pt. II, Chap. 5.
[23] We remark on the measurement of $\underline{S}$ to eliminate possible confusion. The thermopower is measured under zero-current conditions: $\mathbf{J}^e=0$ in Eq. (3). An induced electric field arises given by $\mathcal{E}^{\rm ind}=\underline{S}\nabla T$. But $\nabla T=\nabla T^{\rm ext}+\nabla T^{\rm ind}$ where $\nabla T^{\rm ind}$ is given by Eq. (11) with $J^e_\parallel=0$ and thus for instance the voltage drop along the x direction would be given by $\mathcal{E}^{\rm ind}_x=S_{\rm eff}\nabla T^{\rm ext}$, where $S_{\rm eff}$ is defined in Eq. (13). In an anisotropic medium the matrix elements of the thermopower *cannot* simply be read off from $\mathcal{E}^{\rm ind}/\nabla T^{\rm ext}$; instead, one must measure $S_{\rm eff}$ for several directions and extract from these the individual matrix elements of $\underline{S}$ by inverting the formula for $S_{\rm eff}$ in terms of $\underline{S}$.
[24] C. Herring and E. Vogt, Phys. Rev. **101**, 944 (1956).
[25] R. Ito, H. Kawamura, and M. Fukai, Phys. Lett. **13**, 26 (1964).
[26] A. C. Smith, J. F. Janak, and R. B. Adler, *Electronic Conduction in Solids* (McGraw-Hill, New York, 1967).
[27] L. Esaki and R. Tsu, IBM J. Res. Dev. **14**, 61 (1970).